JOURNAL OF CATALYSIS 123, 130–146 (1990)

Fe–P–O Catalysts for Methane Utilization—Catalyst Development and Identification

ANANTH V. ANNAPRAGADA AND ERDOGAN GULARI[1]

Department of Chemical Engineering, University of Michigan, Ann Arbor, Michigan 48109

Received April 6, 1989; revised January 2, 1990

Fe–P–O catalyst formulations show great promise for oxidative coupling of methane. They attain yields of C_2 hydrocarbons comparable to the best in the literature at a temperature which is far below those reported. The catalysts are active in both supported (on Cab-O-Sil) and unsupported (bulk) forms. Both these forms are active around Fe : P ratios of 0.6, suggesting that the pathway in general is unaltered by the support. The first gas-phase product of the reaction appears to be ethane, which is subsequently converted to ethylene. CO and CO_2 seem to be formed by oxidation of the C_2 hydrocarbons. Activity testing also revealed that a catalyst of this "active composition" was not always active, indicating a possible bifurcation in the reaction rate. The existence of rate hysteresis is confirmed by temperature-programming experiments. ESCA and FTIR studies indicate that the active catalysts are composed of a mixture of various hydrated and unhydrated iron phosphates. These are known to consist of octahedrally coordinated iron atoms alternating with tetrahedrally coordinated phosphorus in phosphate groups. The octahedral coordination of iron includes some direct oxygen links from the phosphates and some indirect Fe–O–H–O–P structures. We speculate that a possible active site for the dehydrogenation is the P–O–P bridge structure of the polyphosphates. We find that on supported catalysts, dehydrogenating species actually build up on the surface during the reaction. These species are specific to dehydrogenation and appear to be incapable of effecting any further oxidation of the products. Thus, gas-phase oxygen alone is responsible for the formation of carbon monoxide and dioxide, while the dehydrogenating oxidic species on the surface are primarily responsible for the formation of C_2 hydrocarbons. This suggests that forced concentration cycling would be a good way of separating products of the reaction on supported catalysts.

INTRODUCTION

The utilization of methane has been identified and targeted as one of the most important challenges facing the catalysis community today. This emphasis is not mislaid either, since enormous amounts of natural gas in remote reservoirs are lying unused due to gas transportation costs and dangers. Conversion of methane to a useful liquid fuel or a more valuable chemical feedstock would thus be an attractive proposition. However, the only commercially used technology today for this conversion is the Mobil process in New Zealand, where a unique combination of economic factors makes the conversion feasible. Elsewhere, the two-step process is not economical. A one-step process converting methane to useful products is thus desirable.

Several compounds have been identified as possible products of such a process. In general, *partial oxidation* of methane refers to the production of methanol and/or formaldehyde, while *oxidative coupling* generally refers to the production of saturated and unsaturated higher hydrocarbons. A comprehensive review of the literature in the area has been carried out by Pitchai and Klier (*1*). In general, partial oxidation of methane takes place at lower temperatures than does oxidative coupling. However, most successful studies on partial oxidation utilize nitrous oxide as an oxidizing agent in

[1] To whom correspondence should be addressed.

0021-9517/90 $3.00

addition to oxygen. This is impractical in commercial situations. Oxidative coupling studies, although conducted at higher temperatures, display significantly higher yields of products. In addition, they utilize oxygen as the oxidizing agent. However, the temperatures at which they operate are still rather high to be commercially attractive. Further, at high temperatures, there is a strong tendency on the part of C_2 compounds to oxidize totally. It seems, therefore, that a catalyst which carries out oxidative coupling at a lower temperature would be the best solution to the problem. (One should note that there are no thermodynamic restrictions to this process; the oxidative coupling process is feasible above 300°K (*2, 3*). The Fe–P–O catalyst formulation we describe below succeeds in doing this. Further, it operates at far higher space velocities than most processes in the literature, a feature which is attractive considering the tendency of C_2 compounds to oxidize totally in the gas phase.

EXPERIMENTAL DETAILS

A. Catalyst Preparation

Two kinds of catalysts were used in this study: unsupported Fe–P–O catalyst of varying Fe : P ratios and the same catalyst supported on Cab-O-Sil HS-5 fumed silica. The catalysts were prepared from ferric nitrate $Fe(NO_3)_3 \cdot 9H_2O$ and an 85% solution of phosphoric acid. The iron salt was dissolved in deionized water and phosphoric acid was added to the solution. The resulting solution was dried at 343°K to prepare the unsupported catalysts. To prepare the supported catalysts, the above solution was used to impregnate fumed silica and the resulting suspension was dried at 343°K.

B. Gases Used

Methane was obtained from Matheson and was 99.99% pure. A gas chromatographic analysis showed negligible amounts of other hydrocarbons in the feed gas. Oxygen was obtained from Air Products and was also 99.99% pure. The diluant or purge gas used was Argon, obtained from Air Products and was 99.998% pure. All gases were used as received.

C. Reactor and Analytical System

The experimental apparatus used consisted of a computer controlled flow manifold which could be connected to a variety of reactors. The basic features of the manifold are described elsewhere (*4*). In short, it contained solenoid valves which were used for flow switching and flowmeters which were calibrated and used to measure the flow rates of the gases during the experiments. Flow rates were varied using needle valves in the lines. Tubing lengths were kept to a minimum to reduce unwanted mixing effects. Two kinds of reactors were used in this study: a U-tube quartz reactor in a constant-temperature furnace, and a straight tube quartz reactor in a temperature-programmed furnace. Both reactors were constructed with quartz tubing of 6 mm outer diameter and normally held 0.1 g of the catalyst between quartz wool plugs.

The constant-temperature furnace had a maximum temperature of 600°C while the programmable furnace could reach temperatures of 1100°C. Consequently, the initial studies were carried out in the constant-temperature furnace, while later studies including temperature programming at high temperatures were carried out in the programmable furnace. Both furnaces had internal control systems.

Quantitative gas analyses were carried out using two gas chromatographs (HP 5710 and 5890). Both GCs were injected with 250 μl of reactor effluent gas simultaneously using inline sample loops on a ten-port sampling valve. One GC was equipped with a flame ionization detector and was used for the analysis of hydrocarbons. The other GC was equipped with a thermal conductivity detector and used for the analysis of carbon monoxide and dioxide. The injection (sampling) valve was triggered by the computer system which controlled the rest of the flow manifold.

Transient gas analysis in real time was done with a quadrupole mass spectrometer (Balzers) connected by a t-flow sample valve to the reactor outlet. The ion current at specific masses corresponding to specific species was calibrated for each run against a GC analysis.

Data acquisition from the GCs was done by two separate integrators (HP 3390 and 3393). Mass spectrometer data acquisition and control was done through our software on the control computer (in this case a HP 9000-300).

ESCA spectra were recorded on a Perkin–Elmer Phi-5800 system. Samples were prepared by pressing 0.1 g of the catalyst into a 1-cm-diameter pellet at 1.06×10^8 Pa. Typical acquisition times were 20 to 60 min, depending on the signal strength. The spectra were referenced to the C_{1s} peak at 284.6 eV.

FTIR spectra were recorded on a Mattson Cygnus FTIR spectrometer. The catalyst samples were diluted in KBr to 5% by weight and 0.1 g of the diluted sample was pressed into a 1-cm-diameter pellet at 1.06×10^8 Pa. Spectra were all referenced against a pure KBr pellet prepared under identical conditions. It should be noted that these spectra were all taken at room temperature, under atmospheric conditions. They need not necessarily reflect the state of the catalyst under reaction conditions. However, as will be seen, they yield significant information.

D. Experimental Details

A catalyst sample (0.1 g) was held between quartz wool plugs in a U-tube reactor and heated at 575°C for 8 h in a stream of oxygen at 50 standard cm^3/min. After this pretreatment, a reaction was run by flowing methane and oxygen through the catalyst bed at a total flow rate of 120 standard cm^3/min and a methane : oxygen ratio of 2 : 1. The total pressure was maintained at 42 psig using a back pressure regulator. Injections were made into the gas chromatographs at specific intervals. Typically, the first was made 5 min after starting the reaction followed by injections at 50-min intervals for the next 10 h. At the end of this period, the reactor was purged with argon at 50 standard cm^3/min while cooling to room temperature. The catalyst was then removed from the reactor and stored for subsequent analysis. Similar procedures were followed to determine the variation of activity with space velocity.

Temperature-programming studies on selected catalysts were carried out by following an identical pretreatment procedure as above. Once the co-feed reaction was started, the desired temperature program was applied to the reactor. Typically this program consisted of 5 min at 575°C, heating at desired rate to desired temperature, maintaining for 1–20 min, and cooling at the desired rate to 575°C.

In one series of experiments, GC injections were made during the initial 575°C period, the high-temperature period, and the final 575°C period. In another series, the product concentration was monitored continuously using the mass spectrometer.

Transient flow experiments (surface titrations) were also carried out. The pretreatment of the catalyst was identical to that mentioned above. Specific flow protocols followed are described along with the results of each transient experiment.

The above catalysts were also removed from the reactor for further analysis.

RESULTS AND DISCUSSION

A. Steady-State Results

The first experiments carried out were activity tests on Fe : P : O catalysts supported on Cab-O-Sil. Figure 1 shows the effect of loading and Fe : P ratio on the C_2 activity of the catalysts. We see that a 4–6% loading is the most active. In addition, a Fe : P ratio of 0.6 seems to be more active than the other compositions.

Typically, 15 samples of each catalyst composition were tested. It was observed

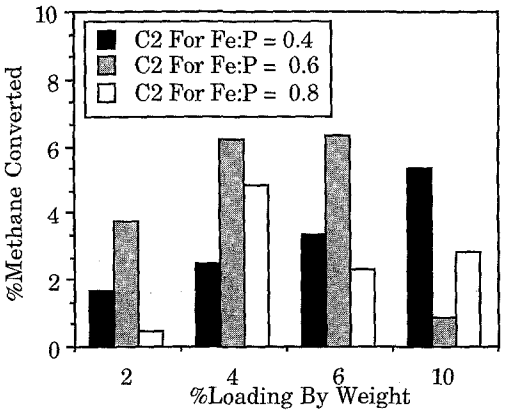

FIG. 1. Effect of catalyst loading and Fe : P ratio on the C_2 yield of supported catalysts. Pressure = 4 atm., temperature = 575°C. Gas flows: CH_4 = 80 standard cm^3/min, O_2 = 40 standard cm^3/min, sample taken after 15,000 s of reaction. Each set of three bars represents three Fe : P ratios at the loading corresponding to the set which is marked on the x-axis.

that the catalysts displayed the activities shown in Fig. 1 about 50% of the times they were tested. During the remaining tests, they displayed extremely low activities (around 0.3% conversion). This led us to believe that a rate bifurcation might exist in some parameter space. It should be noted that the catalyst with this composition at a 10% loading was not active compared to the other compositions. We believe this is because we never attained the high steady state during tests on this catalyst composition.

Steady-state activity measurements were also made on unsupported catalysts of similar composition. Figure 2 shows the results of the study. We see that the catalyst with iron : phosphorus ratio 0.6 is the only active composition. Again, this activity result was obtained approximately 50% of the time, the rest of the trials displaying an activity comparable to the low values consistently displayed by the catalysts of other compositions. We note that the maximum activity in the catalyst composition space occurs at the same Fe : P ratio as that in the case of supported catalysts, suggesting that the active sites and mechanism are basically unchanged by the presence or absence of the support.

The dependence of the activity of the unsupported catalyst on space velocity was also investigated. Figure 3 shows the dependence of fractional selectivity and activity on space velocity at 575°C. We note that at high space velocities, the conversion drops to low values, accompanied by a substantial increase in the selectivity toward ethane (better than 90%). At lower space velocities, the overall conversion increases to a value around 8%, while the ethylene selectivity catches up with ethane. On the other hand, a sizeable amount of carbon monoxide and dioxide are also formed. These results lead us to believe that ethane is the primary product of the coupling reaction and is subsequently dehydrogenated to ethylene and also oxidized to carbon oxides. In addition, ethylene, formed from dehydrogenase of ethane, is also capable of direct oxidation to carbon oxides. As was explained earlier, activity tests on the catalyst samples with Fe : P ratio around 0.6 did not always indicate that the catalyst was active. We surmised earlier that the possibility of multiple

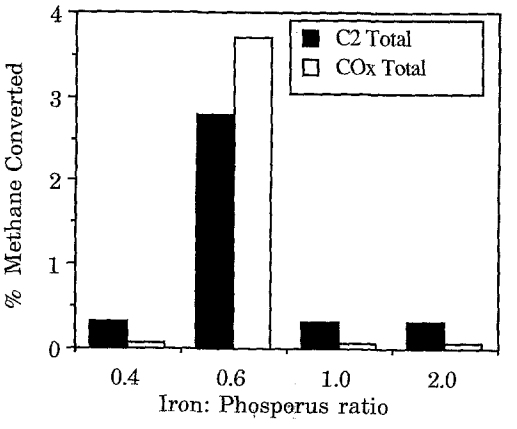

FIG. 2. Effect of Fe : P ratio on the C_2 and CO_x yields of unsupported catalysts. Conditions are the same as those in Fig. 1.

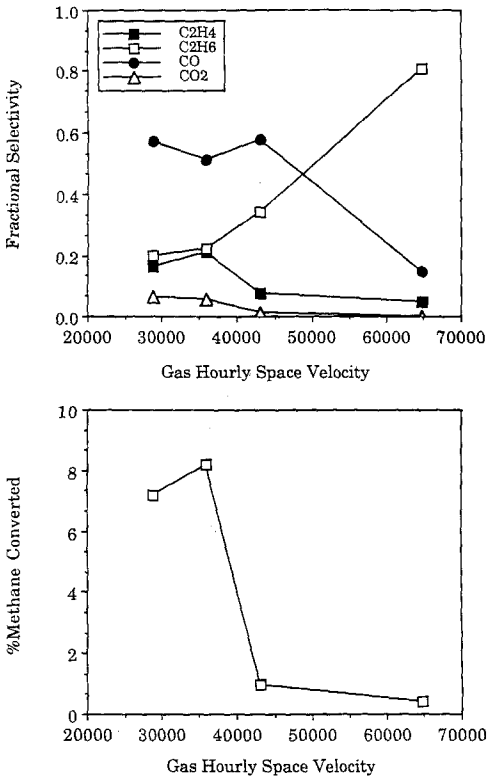

FIG. 3. Effect of GHSV on the C_2 and CO_x yields of unsupported catalyst with Fe : P = 0.6. Sample taken after 5000 s of reaction. Reaction conditions are the same as those in Fig. 1.

steady states in the activity existed. In order to investigate this, we conducted temperature-programmed activation on these samples. The protocol used was as follows:

Load catalyst into reactor and pretreat as usual.

Flow methane and oxygen through the reactor at 575°C. Total flow rate = 120 cm^3/min, 2 : 1 ratio.

Maintain temperature at 575°C for 5 min; inject sample into GC.

Increase temperature to scheduled high value (600 to 725°C) in 30 min.

Maintain temperature for 20 min; inject sample into GC.

Cool to 575°C in 30 min.

Maintain at 575°C for 20 min; inject sample into GC.

The result of this series of experiments are plotted in Fig. 4. As can be seen, the rates during the initial 575°C period were uniformly low. The elevated temperature exhibited rates which were understandably higher. However, on cooling the catalyst to 575°C again, only the samples which were heated to 725°C displayed high activity. All the other samples reverted to their low rate at 575°C. We should point out that the final temperature of 575°C is the temperature measured *inside the catalyst bed.* Cooling of the reactor from the high steady state caused the reaction to revert to the low steady state around 540°C. Subsequent heating of the reactor caused the reaction to map the same path as before, i.e., to remain at the low steady state until 725°C when the high steady state was attained. It was thus concluded that 725°C was the ignition temperature for this hysteresis.

Once we had established this ignition limit, we decided to reevaluate the unsupported catalysts in the light of the new information. We ran temperature-programmed experiments on catalysts with Fe : P ratio around 0.6, keeping the high temperature at

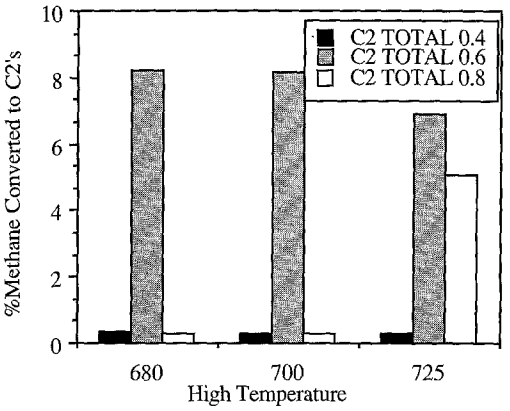

FIG. 4. Identification of ignition temperature in the hysteresis. Each set of bars represents the C_2 yields recorded during (1) the initial period at 575°C, (2) the high-temperature marked on the x-axis, and (3) the final period at 575°C. Catalyst used was silica supported, loading = 6%, Fe : P ratio = 0.6. Heating and cooling rates were 1.5 K/min.

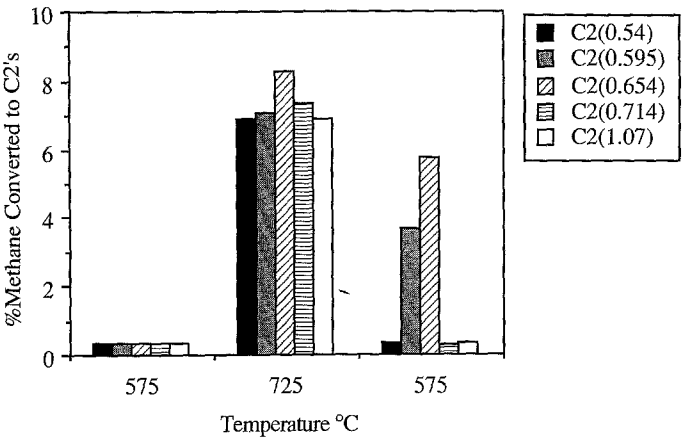

FIG. 5. Evaluation of unsupported catalysts for temperature hysteresis. Each set of bars represents the C_2 yield of the catalyst with the Fe : P ratio shown in the legend at the temperature marked on the x-axis. Heating and cooling rates were 1.5 K/min. Reactor pressure = 4 atm.; flows: CH_4 = 80 standard cm^3/min; O_2 = 40 standard cm/min.

725°C. The results of this experiment are shown in Fig. 5. Again only the catalysts with Fe : P ratios 0.595 and 0.654 were active when cooled to 575°C. This told us that our earlier conclusions about the active range of catalysts still held.

Figure 6 shows the ESCA spectra of (a) an inactive catalyst (Fe : P = 0.4), (b) an active catalyst (Fe : P = 0.6) after a reaction without temperature programming, and (c) an active catalyst (Fe : P = 0.6) after a reaction run with temperature programming. Of these, only sample (c) displayed high activity. All these catalysts were unsupported. Spectra are shown in the Fe_{2p} and P_{2p} regions. As can be seen, the active catalyst displays a shift to lower energies in both regions. The $Fe_{2p_{3/2}}$ peak shifts from 713 to 711 eV and the P_{2p} peak shifts from 134.5 to 133.1 eV. This phenomenon has been observed in the past with phosphates: The shift in the iron peak corresponds to a change-over in the iron from tetrahedral to octahedral coordination (*5*). The shift in the phosphorus peak corresponds to the hydration of phosphates, resulting in an effective HPO_4^{2-} ion (*5*). Structurally anhydrous iron phosphates are essentially similar to silica, with both the iron and phosphorus atoms tetrahedrally coordinated to oxygen. These tetrahedra link together, sharing an edge or a vertex. Hydrated phosphates, however, are somewhat different. The phosphorus remains tetrahedrally coordinated while the iron is octahedrally coordinated to two water molecules and four oxygen atoms belonging to four different PO_4 tetrahedra.

The infrared spectrum of an unsupported catalyst with Fe : P ratio = 0.6 after pretreatment in oxygen is shown in Fig. 7 (curve a), along with the spectrum of the same catalyst after temperature-programmed reaction (curve b). As can be seen, the catalyst that has undergone temperature-programmed reaction shows distinct peaks at 958 and 928 cm^{-1}. Spectra of the same samples in the hydroxyl region are shown in Fig. 8. The active catalyst exhibits a distinct O–H stretch peak at 3450 cm^{-1}.

The spectral features present in Fig. 7 can be attributed to the various characteristic frequencies of the family of iron phosphates. The bands from 1240 to 1100 cm^{-1} were assigned to PO_3 asymmetric stretches, while those from 1080 to 1000 cm^{-1} were assigned to symmetric PO_3 stretches and symmetric and asymmetric stretches of other P–O-containing structures (*6*). The band around 955

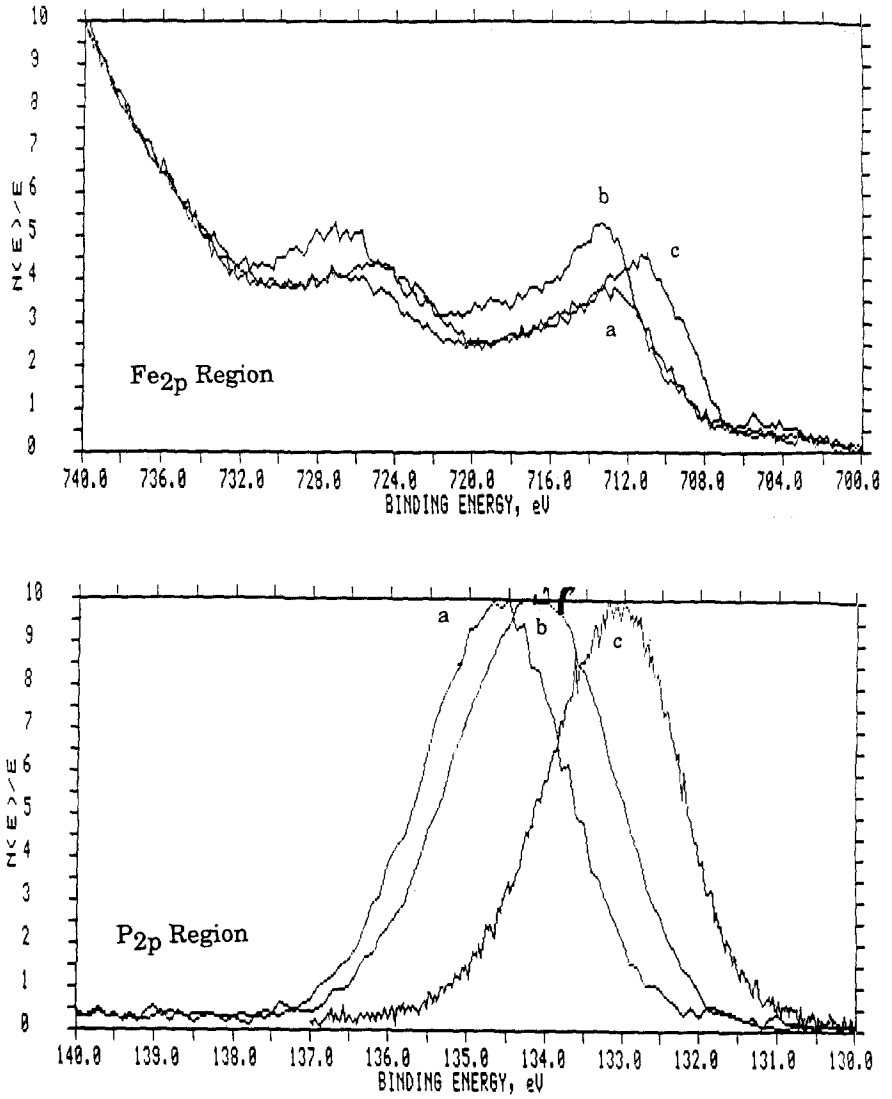

FIG. 6. ESCA spectra of unsupported Fe–P–O catalysts. (a) Fe : P = 0.4, reaction run with temperature programming. (b) Fe : P = 0.6, reaction run at constant temperature. (c) Fe : P = 0.6, reaction run with temperature programming. Catalyst (c) was active, others were not.

cm^{-1} was assigned to a P–OH stretch as in hydrated phosphates, the band at 928 cm^{-1} to the P–O–P asymmetric stretch, and the band at 738 cm^{-1} to the P–O–P symmetric stretch (*7*). In catalysts with low Fe : P ratio, additional P–O stretching bands appear between 770 and 670 cm^{-1}. Such bands have been reported for analogous V–P–O systems (*6*). Bands from 650 to 500 cm^{-1} were assigned to P–O bending vibrations. From the infrared spectra of catalysts in Fig. 7, we can see that the reaction has resulted in the formation of P–O–H structures on the surface. Also, the peak at 928 cm^{-1} corresponding to the P–O–P bridge has become more distinct. The formation of the P–O–H structures is also supported by the peak at 3500 cm^{-1} in the used catalyst, indicating the presence of nonhydrogen-bonded hydroxyl groups on the surface of the catalyst.

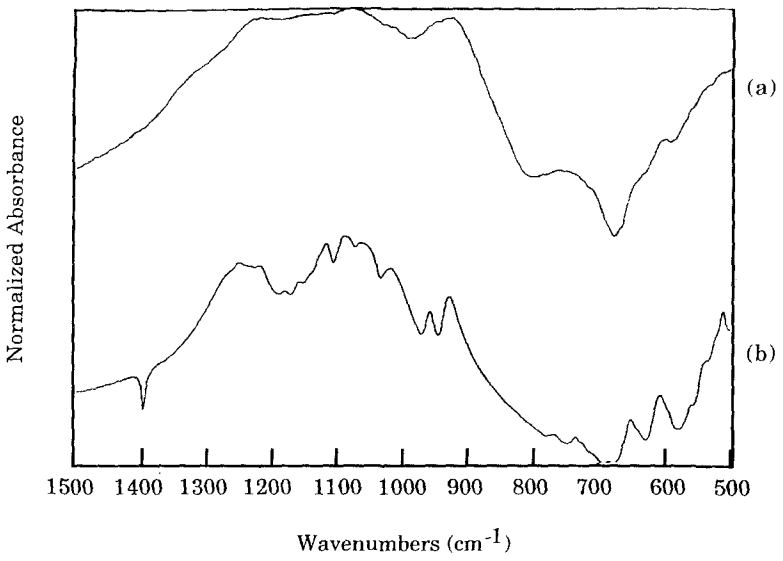

FIG. 7. IR spectra of catalyst with Fe : P ratio = 0.6. Trace (a) before and (b) after reaction with temperature programming. Note the emergence of P–O–P and P–OH structures in the catalyst after the reaction as indicated by the peaks at 928 and 958 cm^{-1}.

The spectra of used catalysts of other compositions showed that these two surface structures coexist only in the active catalysts. This suggests that the hydrogen abstraction process results in the hydrogen being held as a P–O–H group until it is removed as water and that the hydrogen abstraction process takes place on the

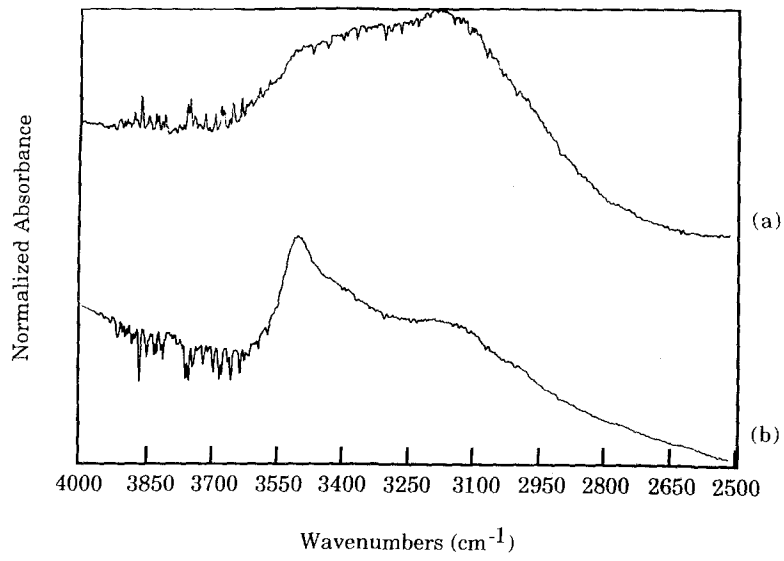

FIG. 8. IR spectra of catalyst with Fe : P ratio = 0.6 (a) before and (b) after reaction with temperature programming. Note the formation of nonhydrogen-bonded hydroxyl groups on the catalyst after reaction indicated by the peak at 3450 cm^{-1}.

P–O–P bridge sites. An alternative explanation could be due to hydration by the water produced during the reaction.

While it is very tempting to accept this as such, it would imply that the P–O–P bridge in general is active for hydrogen abstraction. During activity testing, however, we found that all the pure Fe–P–O materials we evaluated as catalysts for this process (ferric pyrophosphate, for example) were *inactive*. It is possible that some small subset of the P–O–P structures we see is active for the hydrogen abstraction process. In order to probe this, identical catalyst samples of Fe : P ratio = 0.6 were treated with pure CH_4 and pure CD_4 at 575°C. Treating the catalyst with deuterated methane resulted in the appearance of a small O–D peak at 2588 cm^{-1}. The area of this peak is very small ($\ll$1% of the O–H peak in Fig. 8 (trace b)). If we assume that the O–D species is at the location of the active site for the dehydrogenation, then we see that only a very small percentage of sites that are capable of holding a hydroxyl species are also capable of hydrogen abstraction. Further, from the position of the O–D peak and calculation of the isotope shift, we can say that the parent OH species, which is analogous to the O–D must have a signature between 3624 and 3560 cm^{-1}. This is somewhat higher than the position of the O–H peak in Fig. 8b which occurs at 3450 cm^{-1}. Consequently, it appears as if the hydrogen abstraction occurs on only a small number of sites, following which the hydrogen migrates to other sites (corresponding to the band at 3450 cm^{-1}) before being removed from the surface as water.

The magnitude of the isotope shift on the P–OH stretching band can also be calculated and can be shown to result in a peak from 935 to 920 cm^{-1}. Inspection of Fig. 7 shows that this region overlaps with the strong P–O–P band at 928 cm^{-1}. Judging by the strength of the O–D vibration at 2588 cm^{-1}, it seems unlikely that we would be able to see any additional bands in this area. However, we did see a slight shift in the position of the P–O–P band in the deuterated sample to 923 cm^{-1}. This could be accounted for by the presence of an overlapping P–OD band in the region.

B. Transient Response Results

B1. Temperature-programmed reaction (TPR) studies. In order to probe the sequence of events leading to the high conversion steady state we also performed temperature-programmed reaction experiments during which product compositions were monitored in real time.

TPR studies were carried out with the following protocol:

Load and pretreat the catalyst.
Run a co-feed reaction (2 : 1 methane : oxygen ratio, total flow rate = 120 cm^3/min) at 575°C.
Maintain temperature at 575°C for 5 min.
Ramp temperature up to 725°C in 50 min.
Maintain at 725°C for 1 min.
Cool to 575°C in 50 min.

Product detection was accomplished using the quadrupole mass spectrometer system described earlier. In addition, GC measurements were carried out at the end of each temperature period. These measurements were used to check for any changes in the mass spectrometer sensitivity over time. The mass spectrometer traces for mass numbers 15 (methane), 28 (carbon monoxide), 30 (C_2 hydrocarbons), 32 (oxygen), and 44 (CO_2) are shown in Fig. 9.

Initially, from 575°C, the rate of production of C_2 hydrocarbons, CO, and CO_2 is steady, as evidenced by the smooth curves for all the masses. As the temperature is raised, the rate of reaction to all the products increases steadily until an ignition occurs at 16–18 min (625°C). This is evidenced by a sharp increase in the C_2 as well as CO and CO_2 concentrations. We observe that at this point, the C_2 production rate enters a regime of large oscillations. While these oscillations

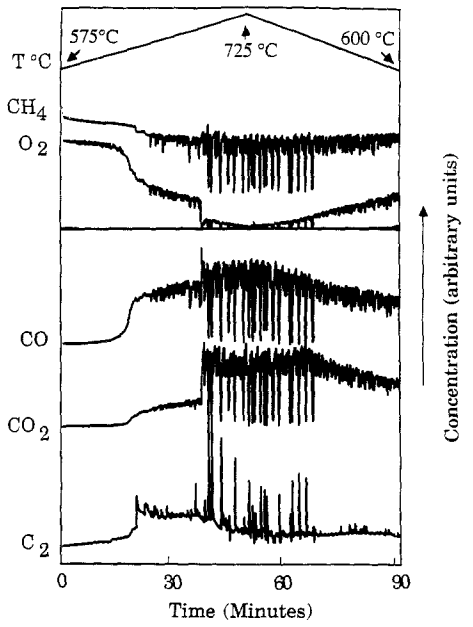

FIG. 9. Mass spectrometer traces during TPR experiment. Temperature profile is described in text.

are significant in magnitude, they are not the largest oscillations this system exhibits. In spite of the existence of the oscillations, it is possible to visually establish a baseline value for the rates, on which the oscillations are superimposed. Closer examination shows that while the oscillations in C_2 values all show increases from the baseline, the oscillations in CO and CO_2 show corresponding decreases. This indicates that the mechanism of the reaction during the oscillations favors the formation of C_2 hydrocarbons in preference to oxidic products. During this phase, the oscillations are also visible in the oxygen and methane traces. It is interesting to note that they are relatively small in the oxygen trace and large in the methane trace. However, they are both in the downward direction from the baseline. Since the stoichiometery for the reactions is

$$2CH_4 + 0.5\,O_2 \rightarrow C_2H_6 + H_2O \quad (1)$$

$$2CH_4 + O_2 \rightarrow C_2H_4 + 2H_2O \quad (2)$$

and for total oxidation

$$CH_4 + 2O_2 \rightarrow CO_2 + 2H_2O \quad (3)$$

$$CH4 + 1.5\,O2 \rightarrow CO + 2H_2O, \quad (4)$$

the total oxidation reactions should consume more oxygen than the coupling reaction. Thus oscillations which display upswings of C_2 products and downswings of CO_x products will cause positive spikes in the O_2 trace. During the oscillations, however, we observe large downward swings in the CH_4 concentration. The high level of conversion of methane in these oscillations should be accompanied by sizeable *negative* swings in the O_2 concentration. However, what we do observe are *small* downward oscillations in the O_2 trace. We believe that the result of the two opposing forces on the O_2 concentration is to cause the small negative swings we observe. As the temperature is further increased in this regime, the methane concentration drops relatively slowly and the C_2 concentration remains roughly constant. The CO and CO_2 concentrations increase steadily. From a stoichiometeric point of view, this is consistent with the observed steeper decrease of the O_2 concentration.

At 38 min (692°C) a second transition occurs. The oxygen concentration drops to very low values, accompanied by a sudden increase in CO_2 concentration. This is stoichiometrically consistent. The slight increase in the mass 28 signal is probably due to CO_2 fragmentation, and the CO concentration does not really undergo a change here. The temperature continues to increase until 50 min where it reaches the programmed maximum of 725°C. This region is characterized by a constant CO_2 concentration with large negative oscillations, constant C_2 concentration with large positive oscillations, constant methane concentration with large negative oscillations, close to complete oxygen conversion with negative spikes going to zero concentration and a

roughly constant CO concentration with negative spikes. While the base conversion values seem to favor CO_2 more than in the previous regime, the oscillations exhibit the same behaviour as before—converting large amounts of methane to C_2 molecules rather than to oxides. We note that for every one of these oscillations, the oxygen concentration has dropped to zero. This suggests that the absence of gas-phase oxygen inhibits the formation of CO and CO_2. The end of this regime occurs at around 70 min (670°C) as evidenced by a sudden halt in the large downswings of CH_4. Note that the remaining downswings in O_2 do not go all the way to zero. Correspondingly, the magnitude of the oxide–hydrocarbon trade-off oscillations also decreases. While the CH_4 concentration remains constant, the O_2 concentration increases gradually. Similarly, the C_2 hydrocarbon concentration remains constant while the oxide concentrations decrease gradually. The end of this region therefore presents a substantially higher rate of C_2 production than that at the same temperature during the first half of the temperature-programmed reaction experiment. This is the high steady state referred to earlier.

The C_2 transient above 625°C on the upswing and on the entire downswing of the temperature program is relatively independent of temperature, except for the rearrangement at 690°C (38 min). This indicates that the mechanism of C_2 production is governed by a physical process (as opposed to a chemical process). Further, the concentrations of oxygen, CO, and CO_2 are all dependent on temperature in this regime, while the concentration of methane is not. This suggests that the physical process governing C_2 production is linked with C_1 species and is probably caused by a physical limitation on C_1 species such as transport to or from the surface. Further, it appears that CO and CO_2 production are not limited by a physical process, and, as such, they are probably formed by total oxidation of the C_2 hydrocarbons. Separate TPR experiments with an empty reactor, as well as with a reactor containing blank support material (results not shown here), showed that in this regime there is a negligible conversion to C_2 hydrocarbons and oxidic products. We conclude therefore that the oxidic products are formed by total oxidation of the C_2 hydrocarbons and that this oxidation occurs in the gas phase. Similar experiments were also carried out at other methane : oxygen ratios. The results were essentially identical to those presented for methane : oxygen ratios varying from 3.5 to 2. At lower ratios, the reaction became explosive and unstable, and further investigation was not carried out. At higher ratios, the high steady state was not attained, possibly due to the smaller amounts of oxygen present. The case of methane : oxygen = 2 has been presented here as a representative of the kinds of dynamic phenomena observed on this system.

B2. Oxygen titration results. The oxygen surface titration was done after 3600 s of high steady-state reaction and a 60-s argon purge. This purge period was required to bring the methane concentration in the gas phase down to zero. The oxygen did not induce any production of C_2 hydrocarbons or CO_x. This shows that during the reaction under the high steady state, there is no detectable carbonaceous species on the surface of the catalyst. The titrations were also carried out for pure methane pretreatment conditions. It was found that the support, the unsupported catalyst, and the supported catalyst had approximately the same amount of carbonaceous deposits. However, the surface area of each of these loads was substantially different: the blank silica had a surface area of 300 m^2/g, the unsupported material 3 m^2/g, and the supported material 160 m^2/g. Consequently, we concluded that the carbonaceous species was not in the form of a monolayer; rather its structure was possibly such that the area of contact with the substrate was minimal, for example, a filamentous species. *In situ* infra-

red experiments were also carried out, and no detectable CH_x species were evident on the surface of the catalyst. Further examination of the infrared spectrum showed no detectable carbonyl species on the catalyst surface either. We thus concluded that the carbonaceous deposits were probably elemental in nature. Such coking of catalytic materials in the presence of carbon-containing gases is well known and is the subject of a number of review papers (*8–10*). More recently, the structure of such materials has been determined by Yang and Chen (*11*), who conclude that the coke is primarily filamentous in nature. In general, however, no carbon of this nature is seen during surface titrations of a catalyst surface under reaction conditions. We conclude therefore that carbon deposition probably does take place even during reaction (co-feed) conditions, but the carbon is not allowed to accumulate; it is oxidized almost immediately in the oxidizing environment of the reaction. This is therefore another pathway to carbon oxides in this system, which appears to go through elemental carbon on the surface of the support.

B3. Methane titration results. Figure 10 shows a typical response from the methane titration experiments. This titration was done after 4 h of reaction in the high steady state following temperature-programmed activation. There was no gas-phase purge, and the experiment consisted of a simple step down of oxygen while the methane flow continued uninterrupted. We note that when pure methane (in the absence of gas-phase oxygen) enters the reactor, it reacts with oxygenated species on the surface, exhibiting the same characteristic oscillatory behavior seen in the high steady-state temperature-programmed experiments. This period lasts for around 450 s of the titration. We also see that after an initial small peak, the oxygen trace has gone to zero for the majority of this period, confirming that this reaction we are seeing is indeed between the introduced methane and the oxygenated

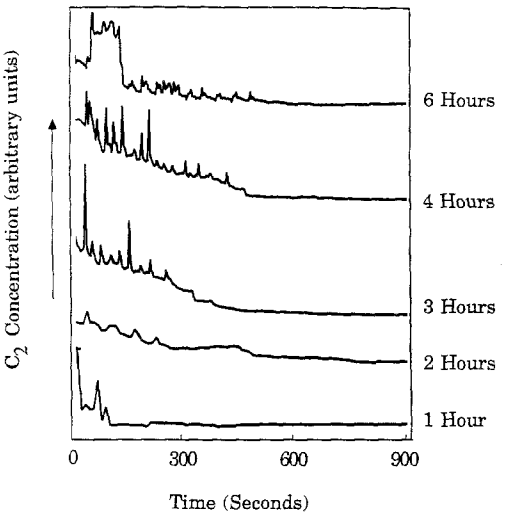

FIG. 10. Methane surface titration after varying times of reaction at high steady state at 575°C. Mass 30 alone is plotted, representing C_2 hydrocarbons.

species on the surface. The CO trace undergoes a baseline adjustment which is understandable during a step change; however, there is no CO being produced during the titration. C_2 hydrocarbons, on the other hand, are being formed, and the trace shows the characteristic oscillations caused by methane mass transfer limitations. After 450 s, the oxygen species on the catalyst surface has been depleted and the methane trace jumps up to a higher value which does not exhibit oscillations.

Similar titration experiments were carried out after 1, 2, 3, and 6 h of high steady-state reaction reached by temperature programming. Each experiment was done with a new load of catalyst in the reactor. We noted that the longer the steady-state reaction time, the larger the area under the decay curve of the C_2 transient. This area is a measure of the amount of C_2 hydrocarbons produced in the reaction and therefore a measure of the amount of oxygen held in the surface dehydrogenating species. The areas under the mass spectrometer C_2 traces were calculated by numerical integration and the amount of oxygen accumulated on the cata-

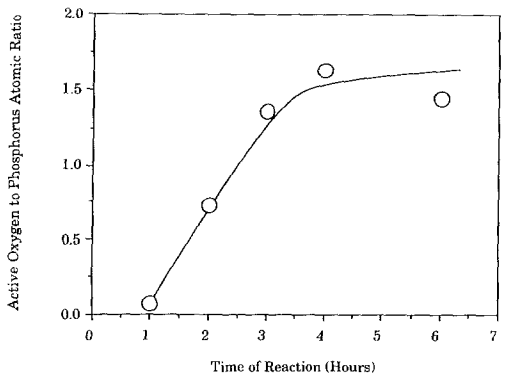

FIG. 11. Active oxygen : phosphorus atom ratio in supported catalyst and accumulation of "oxygen" species at high steady state. Data were obtained from integration of curves in Fig. 10.

lyst was determined. This is shown in Fig. 11, as a plot of the oxygen : phosphorus ratio in the entire catalyst. We see that the amount of oxygen increases up to a time of 4 h and then levels off to a steady state at around a O : P ratio of 1.5.

A variation of the above experiment with gas chromatographic analysis of the products was also done in order to separate the C_2H_4 and C_2H_6 responses. Since the GC analysis took about 3 min, two to three samples were possible during the course of one titration. The experiment was then repeated, with three GC injections during the transient period. From a number of such experiments, the transient could be reconstructed. Since each of these runs required an 8-h pretreatment followed by 5 h of temperature programming and steady-state reaction, we restricted this portion of the study to a steady-state reaction time of 4 h. The results of this transient study are shown in Fig. 12. As can be seen, the C_2H_6 concentration drops to zero in about 450 s after the oxygen flow is stopped. The C_2H_4 and CO concentrations, however, drop to zero relatively quickly (about 90 s). A peak is also visible at 60 s in the C_2H_6 concentration. This is consistent with the postulated mechanism of gas-phase dehydrogenation of the ethane to ethylene. The relatively quick drops in C_2H_4 and CO concentration after the oxygen flow is stopped are also indicative of gas-phase oxidation of C_2 hydrocarbons to carbon oxides. The possibility of C_2 hydrocarbons undergoing combustion is also suggested by the values of ignition tem-

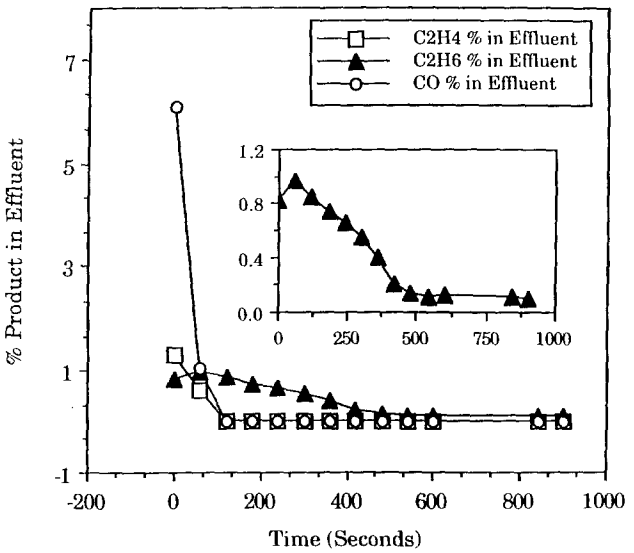

FIG. 12. Methane surface titration of catalyst surface after 4 h of reaction at high steady state at 575°C. Product detection was by GC, enabling separation of C_2H_4, C_2H_6, and CO transients.

peratures of these species in the presence of oxygen. Accepted values in the literature are around 545°C (*12*).

CONCLUSIONS AND SIGNIFICANCE

We have found a new family of catalysts for the oxidative coupling of methane which appear to have great potential. These catalysts consist of novel Fe : P : O formulations which can be supported on Cab-O-Sil fumed silica. The most active catalyst compositions have a Fe : P ratio of around 0.6. These catalysts exhibit, for example, a 15% conversion of methane with a selectivity of 43% to C_2 hydrocarbons at a temperature of 575°C, a pressure of 4 atm, and a space velocity of 28,800 h^{-1}.

The active catalysts exhibit rate hysteresis in temperature space, and the high steady state accounts for the high activity displayed by the catalysts. While this high steady state can be achieved directly from the base temperature of 575°C, the process of doing so possibly depends on local heating in the system to ignite the reaction. A more consistent way of achieving this high steady state is to heat the catalyst to 725°C while running the reaction and then cooling it back to 575°C. Under these conditions, the reaction rate at the final temperature of 575°C is not very different from that at 725°C; in fact, the selectivity is somewhat better. On the basis of the mass spectrometer traces of product transients and the overall catalyst bed temperature measured inside the reactor, we think that the high steady state is occurring isothermally at 575°C and is not due to a hot spot in the reactor but we cannot totally rule out the possibility of high activity hot spots.

From the dependence of selectivity on space velocity, it appears that the first pathway in the reaction is the formation of ethane from methane. Obviously, this ethane has to be formed by the combination of methyl (CH_3-) radicals. The formation of these radicals is accomplished by the dehydrogenation of methane in the presence of oxygen. At low residence times, the high selectivity to ethane indicates that methyl radicals are probably the primary carbon-containing intermediates being formed in the reaction. At higher residence times, ethylene also appears in the products, in addition to sizable quantities of carbon monoxide and dioxide. This leads us to believe that either the ethane is pyrolyzing to ethylene in the reactor or methyl radicals are being oxidatively coupled, i.e., coupling of methyl radicals is taking place after further oxidative dehydrogenation to the methylene (CH_2-) species on the surface. At this point, both hypotheses are feasible. The presence of carbon oxides can be accounted for by the fact that substantial amounts of C_2 hydrocarbons are present in the reactor as a result of coupling, and these are susceptible to total oxidation at the temperatures of the study. It should be noted that the combination of methyl radicals to form ethane in the oxidative coupling reaction over catalysts other than those used in this work has been proposed by Driscoll *et al.* (*13*) and also by Sinev *et al.* (*14*).

While a definite decision between the two routes to ethylene formation cannot be taken at this point, we tend to believe that the first route, viz., the pyrolysis route is more probable. Since the amounts of carbonaceous species on the catalyst surface during reaction under the high steady state are extremely small, it appears that the methyl radicals which are formed on the surface are immediately desorbed from the surface. This has ramifications on the identification of the pathway to carbon oxides too. The relative rates of reactions of methyl radicals have been studied extensively (*15, 16*) and the results have been applied to the case of methane coupling by Lee and Oyama (*17*). According to the calculations presented in the latter work, corrected for our operating conditions, a methyl radical concentration of $>10^{13}$ to 10^{14} cm^{-3} would guarantee that methyl radical coupling in the gas phase would dominate total oxidation reactions of the radicals. In our case, for the conversion figures we see, a methyl radical concentration of 10^{15}–10^{16} cm^{-3} (~1 mol%

under the reaction conditions) would be required. Thus, the possibility that methyl coupling in the gas phase is taking place is not inconsistent with the known rates of reactions involving free radicals. By the same token, it would be extremely unlikely that methyl species which desorb would ever make their way back to the surface for further dehydrogenation to take place. We therefore favor the possibility that ethylene is formed by gas-phase pyrolysis of ethane. Further, it would appear that gas-phase total oxidation reactions to form oxides would have to start from some C_2 hydrocarbon and not from the methyl species. A similar mechanism for the oxidative coupling of methane on silica-supported manganese oxides has been proposed by Sofranko *et al.* (*3*), as well as Lunsford *et al.* (*18*). They too postulate that methyl radicals which desorb into the gas phase will almost definitely combine to form ethane and that ethylene formation occurs only by gas-phase pyrolysis of this ethane. The activity of this catalyst, therefore, can be attributed to its ability to abstract hydrogen from a methane molecule in a controlled fashion and leave the resulting radical species free to undergo further reaction.

We recognize that an oxygen-containing species which is capable of participating in a redox cycle and oxidatively dehydrogenating methane must exist in the system and that this process results in the formation of at least some methyl radicals. Since the formation of one methyl radical from one molecule of methane requires that one atom of hydrogen be abstracted, we need to identify what the initial hydrogen acceptor species is in the system. The hydrogen could be held as a hydroxyl intermediate which is later converted to water. This route would require that the active site be capable of adsorbing and dehydrogenating one molecule of methane. Evidence to this effect is available from the infrared spectroscopy data.

The infrared spectra are consistent with the X-ray photoelectron spectra which indicate the presence of hydrated iron phosphate species during reaction. These hydrated species are known to display a variety of configurations depending on the extent of hydration. A few of the known forms are stengite ($FePO_4 \cdot 2H_2O$), metastengite (same stoichiometry but more open structure), phosphoferrite ($Fe_3(PO_4)_2 \cdot 3H_2O$, ludlamite ($Fe_3PO_4)_2 \cdot 4H_2O$), and vivianite ($Fe_3(PO_4)_2 \cdot 8H_2O$). All these compounds consist of octahedrally coordinated iron atoms alternating with PO_4 tetrahedra. A detailed explanation of these different structures is given in the book by Corbridge (*19*). Any combination of these species could exist in our system. However, from the infrared spectra, the appearance of P–OH and P–O–P bridge species correlate with activity. We therefore speculate that the active site for the hydrogen abstraction reaction is the P–O–P bridge which is broken to form the P–O–H structure during dehydration of the methane. Two P–O–H structures could potentially eliminate a molecule of water between them to form a P–O–P bridge again. However, not all P–O–P structures are active for hydrogen abstraction. Less than 1% of the sites capable of holding a hydroxyl seem to be active for this process.

Several further conclusions can be reached from the transient response data: Temperature-programmed experiments indicate that the reaction undergoes several mechanism changes between 575 and 725°C. These transitions are dependent on the direction of change of temperature. The reaction possesses multiple steady states, and the production of C_2 hydrocarbons is significantly enhanced in the high steady state. This high steady state is characterized by large swings in the reaction rate; these swings are explained by the existence of limiting physical processes. These limitations have been traced to the transfer of C_1 species to or from the surface of the catalyst. Oxygen transfer to the surface of the catalyst is not affected by any such problems. In fact, accumulation of "active oxygen" species on the surface of the catalyst takes

place during the reaction. This accumulation takes about 5 h at 575°C and corresponds to approximately two oxygen atoms for every phosphorus atom. The "active oxygen" species is only formed on supported catalysts and suggests a support interaction with the active component. Since unsupported catalysts are also active, this oxygen donor species is not necessary for activity. It can thus be described as a buffer species which can be converted to the active species. This "oxygen" species as well as the active dehydrogenating site itself are only capable of dehydrogenating methane and do not contribute to ethylene and carbon oxide formation. This is verified by the GC-based titration studies where the ethylene and carbon monoxide concentrations drop to zero relatively quickly in the absence of gas-phase oxygen while the ethane concentration does not. This indicates that the formation of oxidic products takes place in the gas phase only. Thus, generation of the dehydrogenating species on the surface of the catalyst in the absence of methane followed by flowing pure methane over the catalyst should cause pure C_2 hydrocarbons to be formed. The use of this technique to enhance the selectivity of oxidative-coupling processes has been proposed by a number of researchers (*3, 20*) and has been examined by us in another study (*21*) to obtain ethane with >90% selectivity with a time-averaged rate of methane conversion of 3–4%.

In conclusion, we propose a surface reaction scheme as follows: Oxygen induces active dehydrogenating sites, S–O, on the catalyst:

$$S + O \rightarrow S\text{–}O.$$

We have suggested that this site is a P–O–P bridge site in some polyphosphates. On supported catalysts, oxygen also enters into a semi-inert phase from which it can be transported to the active site if needed:

$$O \rightarrow O_{inert} \rightarrow S\text{–}O.$$

These sites abstract hydrogen from methane, forming hydroxyl species on the surface and gas-phase methyl radicals

$$CH_4 + S\text{–}O \rightarrow S\text{–}O\text{–}H + CH_3\cdot.$$

The fate of the hydroxyl species on the surface is as yet unclear, but water is eventually eliminated to regenerate the active sites. We presume this is happening since the activity of the catalyst does not decay for significant periods of time.

Some carbon is deposited on the surface and is immediately removed as carbon oxides in the presence of oxygen.

The gas phase reactions which occur can be summarized as follows:

Methyl radicals combine to form ethane in the gas phase

$$2CH_3\cdot \rightarrow C_2H_6.$$

Ethane undergoes oxidative dehydrogenation to ethylene

$$C_2H_6 + 0.5\ O_2 \rightarrow C_2H_4 + H_2O.$$

In addition, C_2 species undergo total oxidation to CO and CO_2 in the gas phase.

ACKNOWLEDGMENTS

Partial financial support of this research by the University of Michigan and the KCRE program of NSF is gratefully acknowledged.

REFERENCES

1. Pitchai, R., and Klier, K., *Catal. Rev. Sci. Eng.* **28**(1), 13 (1986).
2. Happel, J., and Kramer, L., *Ind Eng. Chem.* **59,** 39 (1967).
3. Sofranko, J. A., Leonard, J. J., and Jones, C. A., *J. Catal.* **103,** 302 (1987).
4. Annapragada, A., Vaporciyan, G. G., and Gulari, E., *Chem. Eng. Sci.* **43**(11), 2957 (1988).
5. Vempati, R. K., Loeppert, R. H., and Cocke, D. L., Paper P-18 presented at the 62nd ACS Colloid and Surface Science Symposium, University Park, PA, 1988.
6. Schrader, G. L., and Wenig, R., *Chem. Eng. Fundam.* **25**(4), 612 (1986).
7. Steger, E., and Kassner, B., *Spectrochim. Acta* **24**A, 447 (1968).
8. Bartholemew, C. H., *Catal. Rev. Sci. Eng.* **24,** 67 (1982).
9. Trimm, D. L., *Catal. Rev. Sci. Eng.* **16,** 155 (1977).
10. Wolf, E. E., and Alfani, P., *Catal. Rev. Sci. Eng.* **24,** 329 (1982).

11. Yang, R. T., and Chen, J. P., *J. Catal.* **115,** 52 (1989).
12. Perry, R. H., Ed., "Chemical Engineers Handbook," 5th ed. McGraw-Hill, New York, 1973.
13. Driscoll, D. J., Martier, W., Wang, J.-X., and Lunsford, J. H. *J. Amer. Chem. Soc.* **107,** 58 (1985).
14. Sinev, M. U., Korchak, V. N., and Krylov, O. V., Paper 124-c4 presented at the International Congress on Catalysis, Calgary, Canada, 1988.
15. Nalbandyan, A. B., and Vardanyan, I. A., *Int. J. Chem. Kinet.* **17,** 901 (1985).
16. Pitz, W. J., and Westbrook, C. K. *Combust. Flame* **63,** 113 (1986).
17. Lee, J. S., and Oyama, S. T., *Catal. Rev. Sci. Eng.* **30**(2), 249 (1988).
18. Lunsford, J. H., and Krylov, O. V., *in* "Proceedings, 9th International Congress on Catalysis, Calgary, 1988" (M. J. Phillips and M. Ternan, Eds.). Chem. Institute of Canada, Ottawa, 1988.
19. Corbridge, D. E. C., "The Structural Chemistry of Phosphorus." Elsevier, Amsterdam/New York, 1974.
20. Bhasin, M. M., and Keller, G. E., *J. Catal.* **73,** 9 (1952).
21. Annapragada, A. V., and Gulari, E., paper 124g presented at the AIChE annual meeting, Washington, DC, 1988.